Accelerated Rupture at the Liquid/Liquid Interface

Tobias Kerle,[†,||] Jacob Klein,*[,†,‡] and Rachel Yerushalmi-Rozen*[,§]

Department of Materials and Interfaces, Weizmann Institute of Science, 76100 Rehovot, Israel, Physical & Theoretical Chemistry Laboratory, Oxford University, Oxford, United Kingdom, and Department of Chemical Engineering, Ben Gurion University in the Negev, 84105 Beer Sheva, Israel

Received April 3, 2002. In Final Form: September 11, 2002

A detailed investigation of a new process of dewetting which takes place at the liquid−liquid interface of partially miscible liquids is reported. We use nuclear reaction analysis and real-time video monitoring to examine in detail the formation of two coexisting liquid films formed by phase separation from a mixture and in particular the subsequent dewetting of one of them from the other. A dewetting front propagates from the edge of the spin-cast sample inward, and it is suggested that a Marangoni flow leads to its initiation and subsequent propagation via a mechanism involving fast rupture of holes ahead of the front. Subsequent growth of holes results in the coalescence of the surrounding rims and their breakup into droplets, whose persistent motion at the interfacial plane is described. This route of dewetting differs from the classical ones involving thermally driven fluctuations or nucleation of dewetting centers, by its relatively short induction time, the evolution of a front, and its unique morphological characteristics. The process is believed to be general and important in thin films of partially miscible liquid mixtures.

Introduction

The lifetime of a thin film formed by forced spreading of a nonvolatile liquid on a noncompatible substrate is an important issue in many technological applications. In particular, for most applications it is required that the relaxation time of the nonstable film would be far longer than the intended lifetime of the product.

Unstable or metastable thin films of a nonvolatile liquid evolve by dewetting. Dewetting is initiated by the rupture of holes and their subsequent growth, leading finally to minimization of the unfavorable film−substrate contact. In these unstable systems, hole rupture is expected to occur via one of two mechanisms, amplification of thermal fluctuations (spinodal dewetting) or heterogeneous nucleation.[1] A common practice in film stabilization is therefore to apply processing conditions that will simultaneously minimize the availability of nucleation centers and block spinodal dewetting. Film preparation in an ultraclean environment and tuning of film thickness often lead to the desired prolongation of film lifetime. While these methods are efficient in blocking the relaxation of single-component films, systems of two or more components may, due to additional degrees of freedom, that is, the free energy being a function of both concentration and interfacial energies, evolve via different pathways leading to a much faster relaxation.

In addition to the classic case of liquid films on solid substrates, the case of liquids on liquids has been receiving much attention in recent years. So far, both experimental studies and theoretical models focused on the investigation of systems of highly noncompatible liquids.[2−6] These studies reported that in the case of highly incompatible liquids dewetting only originates and proceeds via one of the two classical routes: spinodal dewetting or nucleation. The characteristic times for hole rupture scale with the film thickness h as h^{-a}, and the hole growth depends strongly on a single parameter, the viscosity ratio R of the upper to the lower liquid, where $a = 4$ for $R \gg 1$ and $a = 5$ for $R \ll 1$.[7] Thus, while the fluidity of the substrate is predicted to accelerate hole rupture and the growth rate of holes in comparison with dewetting on a solid substrate, it is fundamentally driven by the same interfacial tension that dominates the dewetting of single-component films on a solid substrate.

In cases where the substrate is a thin film of *low* viscosity, compared to the upper layer, it is observed that hole growth is dominated by the fluidity of the substrate. A plug flow evolves and viscous dissipation takes place in the substrate.[5,8] As theoretically predicted,[2] this leads to a much faster rupture than on a solid substrate, while preserving the mechanism of hole growth. However, the evolving morphology and the characteristics of the growth process seem to be general and independent of the rupturing mechanism: At both solid−liquid and liquid−liquid interfaces, the density of holes scales with the film thickness[9] (h) as h^{-4} and a narrow distribution of hole diameters is observed at any given time during the process. It is observed that where the driving force for hole formation is spatially invariant (i.e., in the absence of surface tension gradients in the interfacial plane) the holes form within a narrow time window.

A quite different scenario is expected when the substrate and the film are partially miscible liquids. In this case,

* To whom correspondence should be addressed. E-mail: rachely@bgumail.bgu.ac.il.

† Weizmann Institute of Science.

‡ Oxford University.

§ Ben Gurion University in the Negev.

|| Present address: ContiTech Vibration Control GmbH, Jûdekamp 30, 30419 Hannover, Germany.

(1) Leger, L.; Joanny, J. F. *Rep. Prog. Phys.* **1992**, *55*, 431.

(2) Brochard-Wyart, F.; Martin, P.; Redon, C. *Langmuir* **1993**, *9*, 3682−3690.

(3) Faldi, A.; Composto, R. J.; Winey, K. I. *Langmuir* **1995**, *11*, 4855.

(4) Pan, Q.; Winey, K. I.; Hu, H.; Composto, R. J. *Langmuir* **1997**, *13*, 1758.

(5) Lambooy, P.; Phelan, K. C.; Haugg, O.; Krausch, G. *Phys. Rev. Lett.* **1996**, *76*, 1110.

(6) Stange, T. G.; Evans, D. F.; Hendrickson, W. A. *Langmuir* **1997**, *13*, 4459.

(7) Brochard-Wyart, F.; Debregeas, G.; deGennes, P. G. *Colloid Polym. Sci.* **1996**, *274*, 70−72.

(8) Qu, S.; Clarke, C. J.; Liu, Y.; Rafailovich, M. H.; Sokolov, J.; Phelan, K. C.; Krausch, G. *Macromolecules* **1997**, *30*, 1758.

(9) Brochard-Wyart, F.; Daillant, J. *Can. J. Phys.* **1990**, *68*, 1084.

10.1021/la0203178 CCC: $22.00
Published on Web 11/21/2002

Table 1. Physical Properties of the Oligomers

oligomer	M_w (g mol^{-1})	viscosity (298 K) (P)	T_g (K)
dOS	580	15	250
hOS	2000	glassy	333
OEP	2000	50	213

the composition of the two liquid phases, the thickness of the "substrate" (the lower liquid layer) and the "film" (the upper liquid layer), the geometrical arrangement of the two phases, and the resulting number of interfaces and their location are regulated by the system, rather than being externally imposed. These additional degrees of freedom may lead to a richness of behavior that was not observed before. In the present publication, we present a detailed experimental analysis of the influence of partial miscibility on the dewetting at liquid/liquid interfaces, thus extending our previous brief report.[10]

Thin films of a binary liquid mixture, in the two-phase region of the phase space, evolve spontaneously into two coexisting phases, aligned one on top of the other. Initial conditions which involve spatial concentration fluctuations were found to result in a surface tension gradient near the sample edge. The consequential evolution of a convective Marangoni flow leads to the formation of a dewetting front and fast rupture of holes ahead of the front. This route of dewetting differs from the classical ones and exhibits unique morphological characteristics, as well as a rupture time very much shorter than would be expected from the classical mechanisms. In the following, we describe the process, analyze the observations, and suggest a physical mechanism which is responsible for the phenomenon.

Experimental Section

1. Materials. The oligomers used in the study were fully deuterated oligomeric styrene (dOS) (kindly donated by Dr. M. Wilhelm, Max-Planck Institut fur Polymerforschung, in Mainz, Germany), a higher molecular weight hOS-2K (purchased from Polymer Laboratories, U.K.), and oligomeric ethylene−propylene (OEP) (kindly donated by Dr. L. J. Fetters, Exxon, U.S.A.). The oligomers used are highly monodisperse ($M_w/M_n < 1.04$) Newtonian liquids. Parameters characterizing the physical properties of the two oligomers are presented in Table 1. The styrene/(ethylene−propylene) mixtures have an (upper) critical temperature of about 368 K, as estimated from cloud point measurements. A contact angle of 9° ± 0.5° was measured when a droplet of OEP was placed on a liquid film of dOS and a value of 8° ± 0.5° was measured when a dOS droplet was placed on top of an OEP film, via interference microscopy. The interfacial tension $\gamma_{dOS-OEP}$ can be calculated from the equation $\gamma_{OEP} - \gamma_{dOS-OEP} = \gamma_{dOS} \cos\theta$ where γ_{OEP} is the OEP−air surface tension ($30-33 \times 10^{-3}$ N/m)[9] and γ_{dOS} is the dOS−air surface tension ($29-32 \times 10^{-3}$ N/m).[12] The estimated value of $\gamma_{dOS-OEP}$ is in the range of $(2-3) \times 10^{-3}$ N/m.

Analytical grade toluene (Frutarom or Merck) was used as the solvent.

2. Sample Preparation. Thin films were prepared by spin-casting from a mixture of the components in a common solvent, toluene, at various compositions ($\phi_{OEP} = 0.3, 0.5, 0.7$) on smooth (root-mean-square (rms) roughness as characterized by atomic force microscopy of <2 nm) gold-coated silicon wafers. Double layers were prepared by casting a layer of a pure oligomer (hOS), from toluene, onto a gold-coated substrate, followed by casting of the second oligomer (OEP) from a nonsolvent for hOS (heptane). The heptane does not dissolve the hOS layer previously deposited on the substrate. The overall film thickness was in the range of 80−500 nm. Once cast on the wafers, the films were placed under an optical microscope and monitored under ambient conditions (23 ± 1 °C).

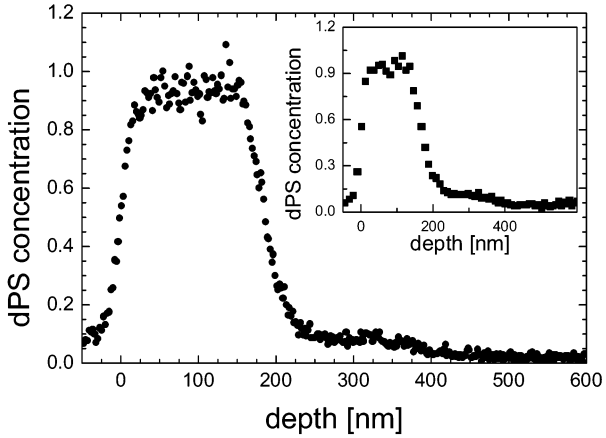

Figure 1. NRA composition−depth profiles of a 400 nm thin film of a dOS/OEP mixture (initial composition of $\phi_{OEP} = 0.5$). The profile presented in the main figure was measured half an hour after coating, and that presented in the inset after 4 h. Although dewetting had already noticeably progressed after 4 h, it was still possible to measure the profile in the as-yet nondewetted, central area of the sample by focusing the profiling ion beam into that area. Both profiles show a dOS-rich ($\phi_{dOS} = 0.9$) layer close to the air surface and a dOS-poor ($\phi_{OEP} \approx 0.1$) layer below.

3. Techniques: Nuclear Reaction Analysis. Composition−depth profiles of the thin films were measured by nuclear reaction analysis (NRA).[13,14] This technique enables the direct measurement of the concentration depth profile of a deuterated species within a nondeuterated environment. In the setup used for the measurements described here, the technique yields a resolution of 10 nm at the sample surface and roughly 30 nm at a depth of 400 nm.

Results

1. Initial Observations. Figure 1 shows NRA depth−composition profiles of thin films, prepared from a symmetric mixture ($\phi_{OEP} = 0.5$) of OEP and dOS. The main figure presents a profile measured half an hour after preparation, and the inset a profile measured after 4 h of annealing at room temperature. The profiles indicate that the films are composed of two layers which differ in their composition, being rich in either one or the other of the respective components. The interface between the layers is aligned parallel to the substrate, as expected for demixed coexisting phases in this thickness range.[15,16] The profiles obtained are identical within the scatter, which indicates that the steady state with respect to composition was reached within less than half an hour.

In Figure 2a−c, we present a sequence of images (optical microscopy) of a dewetting film (400 nm, symmetric dOS/OEP mixture). A dewetting front advances from the edges of the sample which, as the interference colors show, are clearly thicker than the rest of the sample, for example, Figure 2a. Figure 2b shows a typical intermediate stage of the process: droplets are forming at the outer regions of the films, while the middle area of the sample remains visually smooth and unperturbed. The time required for reaching this stage strongly depends on the initial film thickness. Eventually, the stage shown in Figure 2c is reached (after a time $\Delta t \approx 850$ min for the film shown

(10) Yerushalmi-Rozen, R.; Kerle, T.; Klein, J. *Science* **1999**, *285*, 1254.
(11) Fetters, L. J. Private communication.
(12) Gains, G. L.; Le Grand, D. G. *Colloids Surf., A* **1994**, *82*, 299.
(13) Kerle, T., et al. *Acta Polym.* **1997**, *48*, 548−552.
(14) Chaturvedi, U. K., et al. *Appl. Phys. Lett.* **1990**, *56*, 1228−1230.
(15) Binder, K. *J. Chem. Phys.* **1983**, *79*, 6387−6409.
(16) Scheffold, F., et al. *J. Chem. Phys.* **1996**, *104*, 8786−8794.

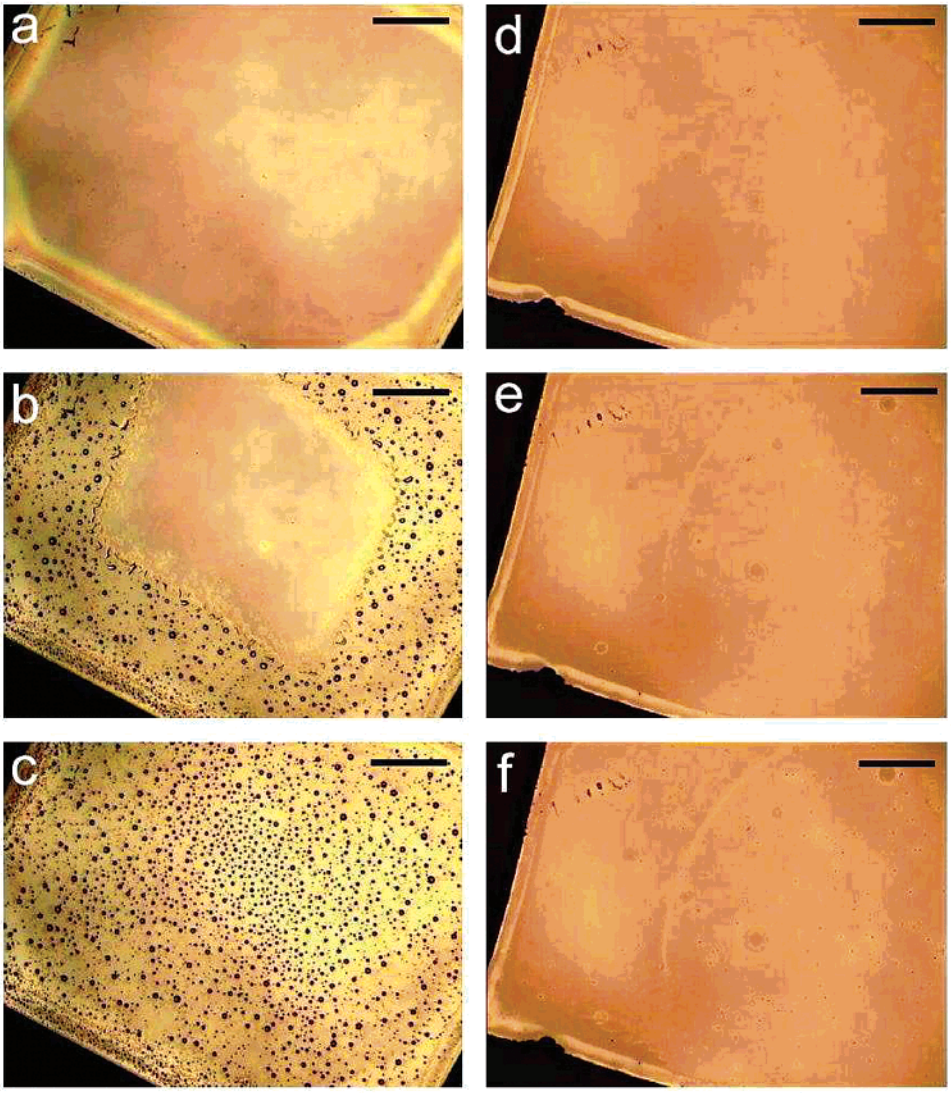

Figure 2. Optical images of a mixture of a dOS/OEP mixture ($\phi_{OEP} = 0.5$) (a−c) and bilayers (d−f) cast on a gold-coated silicon wafer from a toluene solution. The bilayers were formed by casting a 200 nm thick dOS film on top of a 200 nm thick OEP film. Scale bar is 2.5 mm. (a−c) Time evolution of dewetting in an initially 400 nm thick film. (a) Immediately after preparation; (b) the film after $\Delta t \approx 270$ min; (c) the film after $\Delta t \approx 850$ min; (d) bilayer immediately after preparation; (e) the bilayer 5 h after annealing at room temperature; (f) 26 h after coating of the bilayer.

here). At this point, large fractions of the sample surface are covered with droplets, whereas the region close to the sample edges is relatively depleted of droplets, in comparison to the inner parts of the sample. A higher magnification of the front region observed in Figure 2b is presented in the inset to Figure 6. The rupture of fresh holes is observed in an area that typically extends up to a few tenths of a millimeter ahead of the advancing rim. The characteristic hole size clearly decreases away from the front, toward the center of the sample. Note that the freshly formed droplets reveal a round contact line, indicating that the droplets equilibrate rapidly.

A similar dewetting behavior (not shown) was observed in films of dOS/OEP mixtures prepared from different initial compositions, that is, $\phi_{OEP} = 0.3$ and $\phi_{OEP} = 0.7$ blends.

To test the role of the initial sample configuration in the observed phenomenon, we prepared bilayers of the pure components, OEP and OS, on top of gold-covered silicon wafers in a two-step process: A 200 nm thick film of hOS was spin-coated onto a substrate from a toluene solution. Subsequently, a second 200 nm thick layer of OEP was coated on top of the hOS film from the selective solvent, heptane (which does not dissolve or solvate the styrene oligomer). A typical bilayer sample is presented in Figure 2d−f. The temporal evolution of the bilayers clearly differs from the evolution of the films cast from a mixture (Figure 2a−c): 26 h after coating, a time when the mixed layer is already completely dewetted (Figure 2c), the surface of the bilayer is still visually smooth and shows no indications of holes (Figure 2f). A 10 times higher magnification (not shown) reveals that the sample surface looks slightly pocked, thus indicating the initiation of dewetting at the *solid−liquid* interface, probably due to nucleation of holes.

2. The Role of the Different Parameters. 2.1. The Effect of Surface Energy. It is known that the surface energy of a deuterated hydrocarbon is lower than that of its nondeuterated analogue. To test the role of surface energies, we prepared thin films from a symmetric mixture ($\phi_{OEP} = 0.5$) of two nondeuterated oligomers, hOS and OEP, following the procedure described above. We observed that the hOS/OEP films evolved via a dewetting process similar to the one presented in Figure 2a−c. The dewetted layers were then rinsed with heptane which selectively dissolves OEP. This led to dissolution of the

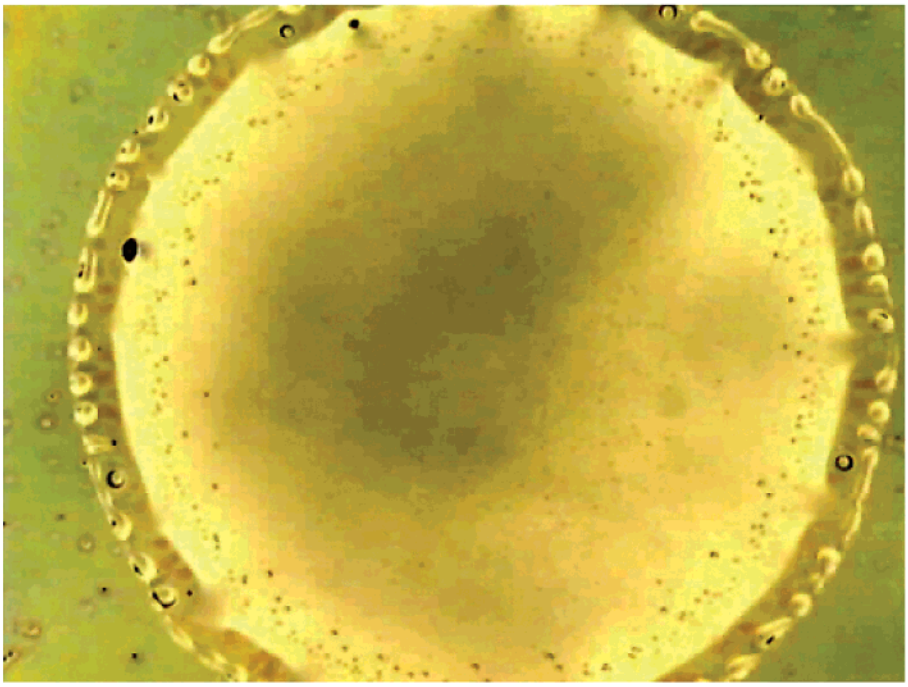

Figure 3. An image of a droplet of OEP (the dimensions of the image are 1 cm by 1.5 cm) placed at the central region of a thin dOS/OEP film (520 nm thick, $\phi_{OEP} = 0.5$). Note the propagation of a front beginning from the droplet outward.

droplets, leaving a layer of finite thickness (in the range of 100−200 nm, as indicated by the interference colors) on top of the silicon wafer. The selective dissolution indicated that in the hOS/OEP mixture the layer at the air interface is the OEP-rich phase.

2.2. Liquid versus Solid Subphase. The role of the fluidity of the subphase in the dewetting process was investigated by replacing the low molecular weight OS of the hOS/OEP mixture with a styrene oligomer of higher molecular weight, hOS-2K ($M_w = 2000$). This material has a glass transition temperature of $T_{g,hOS\text{-}2K} = 333$ K, which is below the critical temperature of the hOS-2K/OEP mixture. The symmetric blend of hOS-2K/OEP was coated on a gold surface and annealed at 338 K. Dewetting behavior similar to the process shown in Figure 2 was observed. In a different experiment, a thin film of a symmetric blend ($\phi_{OEP} = \phi_{hOS\text{-}2K} = 0.5$) was annealed for a few hours at a temperature of 338 K ($> T_{g,hOS\text{-}2K}$). However, after the dewetting had started and the dewetting front was already progressing inward, the sample was quenched to 323 K ($< T_{g,hOS\text{-}2K}$). Although only the lower layer, that is, the hOS-2K, solidifies at that temperature and the change in the OEP viscosity due to the temperature change is negligible, we observed a clear "freezing" of the dewetting process. Heating to 338 K renewed the propagation of the dewetting front. Repeated cycles of temperature elevation and reduction resulted in reproducible freezing/unfreezing transition.

2.3. Sample Edges. In thin films which are prepared by spin-coating, sample edges differ from the bulk by two variables: thickness and local concentration. As both thickness and concentration fluctuations influence the dewetting process, we performed experiments in which the two parameters were decoupled: A shallow scratch was made in the center of a freshly coated film of a symmetric dOS/OEP mixture. Due to the scratching, a liquid rim developed at the borders of the scratch with a thickness comparable to that observed at the sample edges. In a second experiment, a droplet of OEP was placed at the central region of a thin dOS/OEP film. In this configuration, the pure OEP droplet is surrounded by a region of almost-pure dOS, leading to the formation of a compositional gradient in the plane of the sample. In this second experiment, we observed the beginning of an evolution of a dewetting front, which propagated away from the droplet toward the edges of the sample. A typical image of a dewetting front induced by a droplet of pure OEP can be seen in Figure 3. A comparable front did not evolve in the "scratch" experiment.

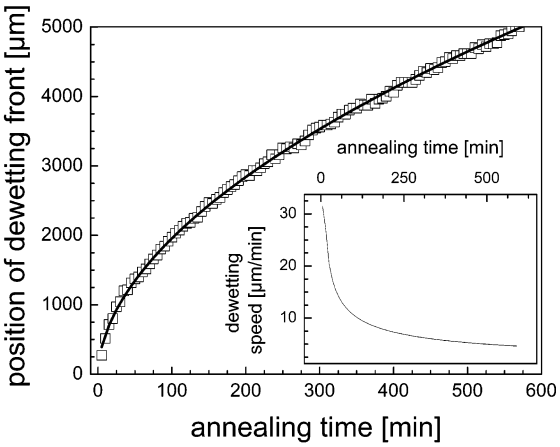

Figure 4. Average distance of the dewetting front from the sample edge as a function of time. The inset shows the derivative, i.e., the velocity of the dewetting front as a function of time, as calculated from a fit to the experimental data. Following an initial period of $\Delta t \approx 150$ min where the propagation speed v_p decreases rapidly, the front velocity decreases with time. The solid curve through the data is a best-fit guide to the eye.

3. Analysis of the Dewetting Process. In Figure 4, we present an analysis of the temporal evolution of the dewetting front. The average displacement of the dewetting front from the sample edge and the corresponding dewetting velocity (inset) are plotted as a function of time. During an initial period of $\Delta t \approx 150$ min, the propagation speed decreases rapidly, to a terminal value at the sample center. The analysis in the discussion section suggests that the time variation of the front propagation may be

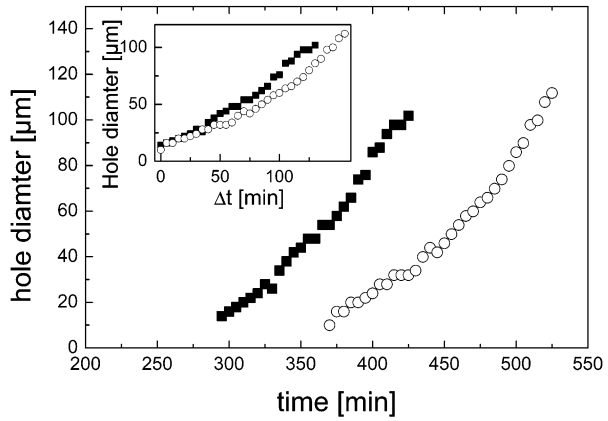

Figure 5. The hole diameter as a function of time, for two different holes, measured in a 400 nm thick dOS/OEP film ($\phi_{OEP} = 0.5$). The inset shows the growth behavior of the same two holes using the time interval as a common *x*-axis.

understood in terms of a radial compositional variation arising from the spin-casting process together with the different viscosities of the two liquids. While the initial dewetting front velocity of similar samples (with respect to composition and thickness) frequently varied by up to a factor of 3, the terminal velocity was always comparable and when reaching the central region of the sample was about 5 μm/min. The large variance in the initial velocity may be due to the relatively large experimental scatter in the front position resulting in large variations in the initial slope of the *x* versus *t* plot.

Figure 5 shows the growth with time of holes. Data for two different holes are shown. We follow the holes up to the stage where the growth is perturbed either by coalescence with neighboring holes or by the dewetting front. The growth rate is characterized by an induction period, which depends on the location of the hole with respect to the sample edge, followed by an increasing velocity. We note that the observed growth velocities are 1−2 μm/min, always lower but of the same order of magnitude as the terminal velocity of the dewetting front.

Figure 6 presents the average hole diameter as a function of the distance from the dewetting front, as obtained from an analysis of micrographs such as that shown in the inset. The position dependence of the hole size differs significantly from the nearly monodisperse distribution of hole sizes which characterizes dewetting processes in single-component films.[17,6] At a given distance from the front, the size distribution of the holes is rather narrow (as indicated by the bars), suggesting that at a given region holes form during a narrow time window.

In Figure 7, we plot the droplet size distribution at the steady state (presented in the inset). We find that the number of droplets in a projected area decays exponentially with the droplet diameter.[18]

Figure 8 demonstrates the redistribution of mass in the upper layer, occurring during the dewetting process. In Figure 8a, the thickness distribution across the as-cast oligomer film of the symmetric dOS/OEP mixture (measured by ellipsometry) is presented schematically. Apart from the sample edges, where one can observe a rim of overall height $h_{rim} = 450$ nm, the film is flat and varies by less than 5 nm from the average film thickness of $h_0 = 400$ nm. In the sample analyzed here, the rim extends roughly 500 μm from the sample edges. In general, this lateral extension depends on the viscosity of the spin-coated mixture, the evaporation rate of the solvent, and the rotation rate while coating. The distribution of droplets at the final stage of dewetting is shown in Figure 7. The volumes of all droplets within strips of 450 μm width, parallel to the sample edge, were integrated. The histogram of Figure 8b presents these integrated volumes in arbitrary units plotted as a function of the distance from the edge. Comparison of the initial film thickness (Figure 8a) with the thickness distribution presented in Figure 8b clearly indicates that a mass transport from the edges inward has occurred.

Discussion

In this study, we report the observation of a process of dewetting at the liquid−liquid interface of partially miscible liquids: When submicron thick films of partially miscible liquid mixtures are prepared in the two-phase region of the phase diagram, they spontaneously equilibrate by separating into the two coexisting phases. The experimentally imposed asymmetric boundary conditions result in the alignment of the two liquid phases parallel to the substrate, where the component with the lower value of the surface energy is found at the liquid−air interface. When the interfacial tension between the two liquid layers, γ_{AB}, is higher than the difference between the air−liquid interfacial tension of the two, $\gamma_{AB} > \gamma_{AV} - \gamma_{BV}$, the resulting bilayer structure is metastable and expected to evolve by dewetting of the upper layer. The lifetime of the configuration is determined by the height of the kinetic barrier for dewetting of the upper layer. The major observation of this study is that in the system investigated by us, a novel pathway of dewetting may be triggered by the initial conditions, offering an alternative, faster route to the classical dewetting pathways.

In the following, we discuss the process in terms of a three-stage mechanism: front initiation, front propagation, and hole formation and growth. The hole growth process ultimately leads to the coalescence of the rims of adjacent holes and their breakup into droplets.

1. Initiation of the Dewetting Front. The most striking feature of the presented process is the evolution of a front, which progresses simultaneously from all sample edges inward. In this system, the edges are distinguished from the central region of the film by their thickness and composition (Figure 9): the local thickness of the edges is significantly higher than that of the middle region (h_0), leading to the formation of a liquid-rim, and the composition of the rim region is enriched by one of the components (due to differences in viscosity and solubility in the carrier solvent). In the case of dOS/OEP, the rim is enriched by the OEP oligomer. Our investigation, and in particular the observation that a droplet of pure OEP located at the center of the film initiates a dewetting front which propagates from center outward, indicates that a compositional gradient can serve as a trigger for the initiating of a dewetting front.

It is well-known[20,21] that in-plane compositional gradients, which result in the formation of spatial interfacial tension gradients, may initiate a hydrodynamic convective flow, known as the "Marangoni effect". From a macroscopic

(17) Jacobs, K.; Herminghaus, S.; Mecke, K. *Langmuir* **1998**, *14*, 965−969.

(18) Towards very small droplet sizes, the data deviate significantly from the exponential dependency due to the finite resolution of the CCD camera used.

(19) A similar rinsing of the dOS/OEP film with heptane removed the whole dewetted structure, indicating that OEP is the lower layer in these samples. This observation is consistent with the layering as observed by NRA.

(20) Linde, H., et al. *J Colloid Interface Sci.* **1997**, *188*, 16−26.

(21) Fanton, X.; Cazabat, A.-M. *Langmuir* **1998**, *14*, 2554−2561.

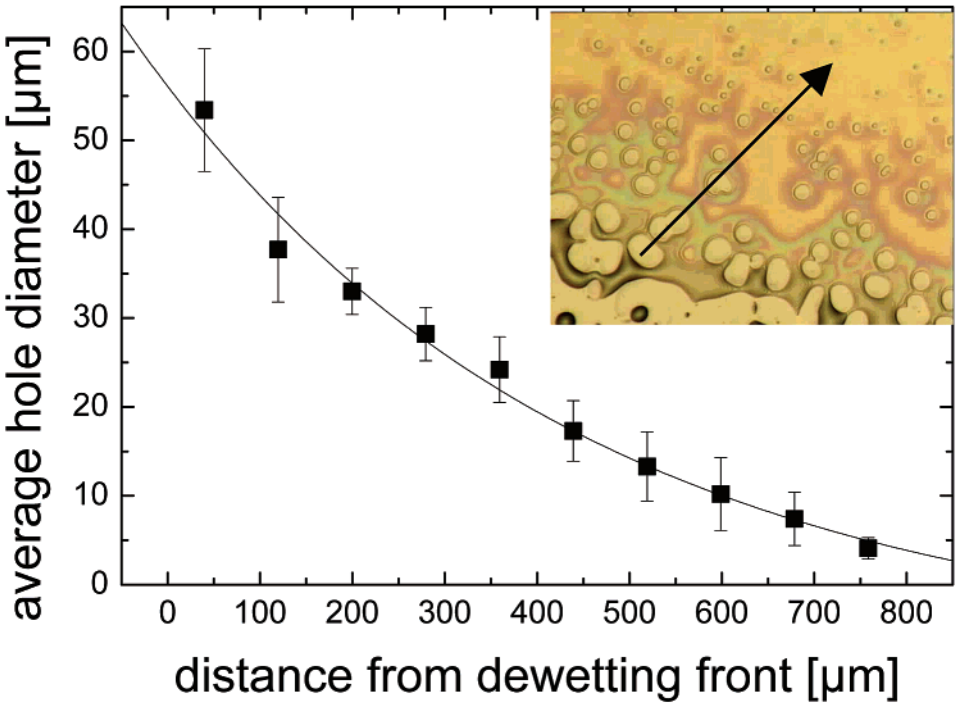

Figure 6. The average diameter of the holes as a function of the distance from the dewetting front. To calculate the average hole diameter, all holes within 90 μm strips were measured. The statistical deviation σ is shown as bars. The inset presents a higher magnification (×10) of the front regime presented in Figure 2b.

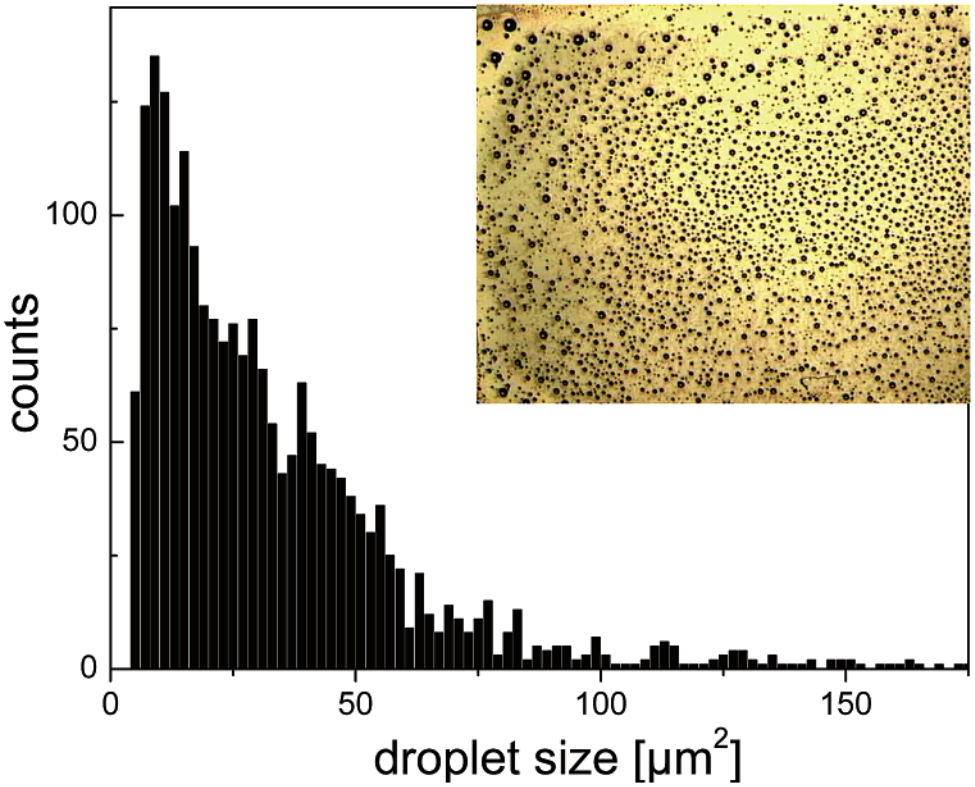

Figure 7. Distribution of droplet diameters in a dewetted film of dOS/OEP (thickness, 350 nm; composition, $\phi_{dOS} = \phi_{OEP} = 0.5$).

point of view, the gradient produces a shear stress, that induces motion in the interface and in the liquid layer in its vicinity, leading to a mass transfer at a rate which is determined by the balance between the radial surface tension gradient ($d\gamma/dx$) and the shear stress. For a planar surface and an upper film of thickness h, the shear velocity V_M of the liquid (of viscosity η) moving from the sample edge inward is described by eq 1.

In the system presented here, h (the thickness of the upper film as measured by NRA) = 200×10^{-9} m, η (the viscosity of the major component of the upper film, dOS in our case) = 15 P = 1.5 Pa s, $d\gamma_{dOS-OEP}$ (the estimated interfacial tension between the two oligomers) = $(2-3) \times 10^{-3}$ N/m, and dx (estimated from the width of the rim, as measured by ellipsometry) = 0.5 mm = 5×10^{-4} m. Putting the values into eq 1 gives V_M = 16−24 micron/

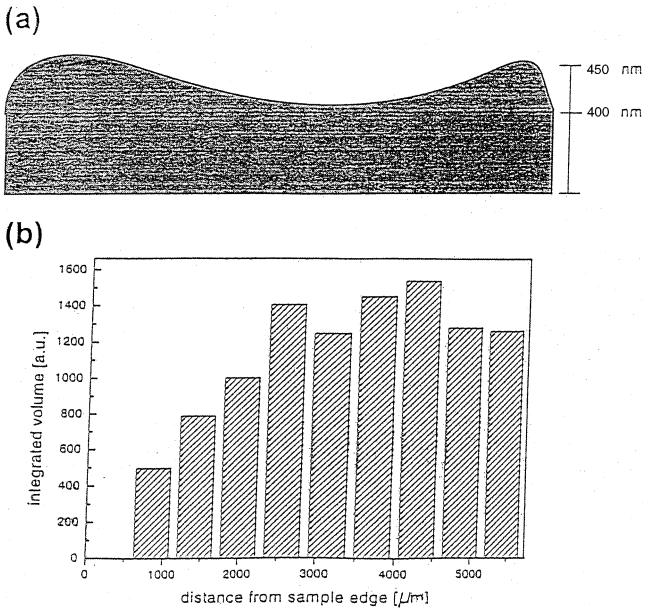

Figure 8. (a) A schematic representation of the thickness distribution in freshly cast films of a symmetric dOS/OEP mixture, as measured by ellipsometry. (b) Integrated droplet volume in 450 μm wide strips as a function of the distance from the sample edge.

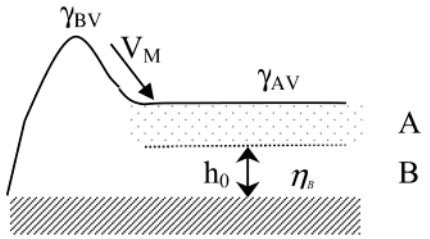

Figure 9. An illustration of the initial conditions leading to the onset of a Marangoni flow. An OEP-rich rim is in contact with the two coexisting phases (the upper layer, A, is dOS rich, while the lower layer, B, is rich in OEP). The resulting gradient in interfacial energies at the rim region leads to the onset of a flow, with a velocity V_M.

$$V_M = (h/2\eta)(d\gamma_{dOS-OEP}/dx) \quad (1)$$

min (slightly higher than the estimation given in ref 10), which is comparable to the observed initial velocity of the front.

The flow results in a mass transfer in the interfacial plane (as described in Figure 8), from the edges inward, finally leading to depletion of material from the outer 2000 μm. The material accumulates as droplets in the inner region and presumably is enriched by dOS.

Our suggestion that a Marangoni flow serves as a trigger for the initiation of the dewetting process described in this study is supported by two additional observations: (1) The process can be inhibited by preparing the system in the two-layer configuration, where each of the layers is cast from the pure component. This procedure prevents the formation of an in-plane compositional gradient. (2) Previous studies of dewetting at the liquid−liquid interface,[3−7] which were carried out in model systems of highly nonmiscible polymeric bilayers in a configuration similar to our "bilayer" samples, Figure 2d−f, did not observe the mechanism reported here. Indeed, a Marangoni flow requires finite miscibility of upper liquid in the lower subphase.[22]

2. Propagation of the Dewetting Front. Following the stage in which the dewetting front is initiated at the sample edges, it advances beyond the rim toward the central region of the sample. The propagation mechanism of the front appears to be similar to that of the growth of holes in the classical processes of dewetting. In both cases, the driving forces have capillary and gravitational components (the latter are negligible in our case), and dissipation is due to frictional processes. For the case of a liquid dewetting from a thin liquid substrate film, we expect that the dissipation is mainly a viscous one in the substrate film itself. Following the model of Brochard-Wyart et al.,[7] the driving force per unit length of the dewetting front will be given by the local spreading coefficient S:

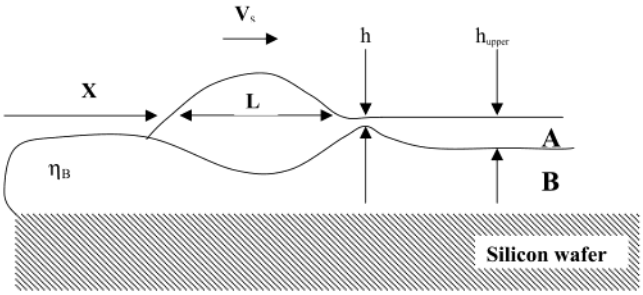

Figure 10. An illustration of the mechanism suggested for the progress of the front. The motion of the liquid rim leads to local thinning of the upper layer; as the rim begins to move, its flow distorts the lower film, leading to the formation of a wave of the lower liquid.

$$S = \gamma_{AB} + \gamma_A - \gamma_B \quad (2)$$

where γ_{AB} is the interfacial tension between the two liquids and γ_A and γ_B are the surface tensions of the upper and lower liquids, respectively.

As seen in Figure 4, the motion of the dewetting front is initially rapid and slows down at later times as it reaches the sample center. A detailed investigation of the dynamics of liquids spreading on liquid substrates has been presented by Joanny,[23] but our conditions are somewhat different to his configuration, and we analyze them using the model illustrated in Figure 10. This shows the top dewetting liquid layer (A) at time t when it has advanced by an extent x from the edge of the sample (where $x = 0$); a rim of width L has formed and is moving as shown at velocity V_s, where

$$V_s = dx/dt \quad (3)$$

The work (dW/dt) done by the dewetting front moving from left to right as shown in Figure 10, per unit time per unit length of the front, is given by

$$|dW/dt| = V_s\Delta\gamma \quad (4)$$

where $\Delta\gamma$ is the energy change per unit area of exposed surface of the lower film, which equals the local value of S, the spreading coefficient.

We may assume that the viscous dissipation takes place primarily within the volume of the lower film underneath the rim area (since $L \gg h_0$, the thickness of the lower liquid film). The volume per unit length of dewetting front is Lh_0, and the rate of energy dissipation per unit volume is $(V_s/h_0)^2\eta_B$, where η_B is the viscosity of the lower film, B.

(22) Adamson, A. W. *Physical Chemistry of Surfaces*; Wiley: New York, 1994.

(23) Joanny, J. F. *Phys. Chem. Hydrodyn.* **1987**, *9*, 183−196.

Thus equating the work done by the moving front to the energy dissipated underneath the rim, we have

$$V_s \Delta\gamma = (V_s/h_0)^2 \eta_B L h_0 \quad (5)$$

giving

$$V_s = (\Delta\gamma h_0)/(\eta_B L) \quad (6)$$

If we were dealing with an unbroken rim whose volume is the accumulated liquid from the region x to the left of the moving dewetting front, then we would expect $L \approx x$. In that case, substituting eq 3 into eq 6 and integrating, we find that

$$x = (2\Delta\gamma h_0/\eta_B)^{1/2} t^{1/2} \quad (7)$$

and

$$V_s = dx/dt = (\Delta\gamma h_0/2\eta_B)^{1/2} t^{-1/2} \quad (8)$$

The data in Figure 4 do indeed show a variation which is close to $t^{1/2}$ and $(1/t^{1/2})$ for the position and the velocity of the dewetting front, respectively. However, as seen clearly from the inset of Figure 6, in our system the rim continuously drains into droplets, so that L remains roughly constant, *not* proportional to x. The origin of the slowing down in the front motion must therefore lie elsewhere. Examination of eq 6 suggests this decay in V_s may be due to variations in h_0 or a gradient in $\Delta\gamma$ as the front proceeds.

3. Hole Formation and Growth. We observed that during the process holes rupture ahead of the dewetting front. We recall that the interface between two liquid layers is deformed by flow within the upper layer when liquids of comparable viscosities, or a top layer of higher viscosity, are present.[2,4,24] It was observed[8] that a rim moving at the liquid/liquid interface pushes ahead an elevated lump of liquid, creating a crest of the lower liquid, as illustrated in Figure 10. The parameters governing the height of this crest are the velocity of the rim, the coupling between the two layers (i.e., the ratio of the two viscosities), and the deformability of the interface, which depends on the interfacial tension $\Delta\gamma$. As the interfacial tension between the two coexisting liquid phases investigated here is very small, the interface is highly deformable. The value of the surface tension at the liquid−air interface is substantially higher. Therefore, the local deformation of the interfacial plane leads not to undulations of the upper surface but rather to local thinning of the upper layer whose initial thickness is h_{upper}. A thickness $h < h_{upper}$ forms a zone of higher rupture probability (recalling that for a fluctuation-driven dewetting process the rupture time, τ, scales with the film thickness as $\tau \sim h^5$ for dewetting on a high-viscosity sublayer and $\tau \sim h^4$ for a lower viscosity subphase).[7,23] We tentatively suggest that a line of "preferred breakup points" ahead of the dewetting front forms by the mechanism suggested in Figure 10. This mechanism is consistent with the locally narrow distribution of hole diameter and the quenching of the process due to a solidification of the substrate (as described in the results): The propagation of a crest creates regions of reduced thickness at a well-defined distance ahead of the front. The width of the distribution of hole diameter is then a consequence of the residence time of the crest at any given point, which is determined by the velocity of the propagating front. This idea is further supported by

(24) Segalman, R. A.; Green, P. F. *Macromolecules* **1999**, *32*, 801.

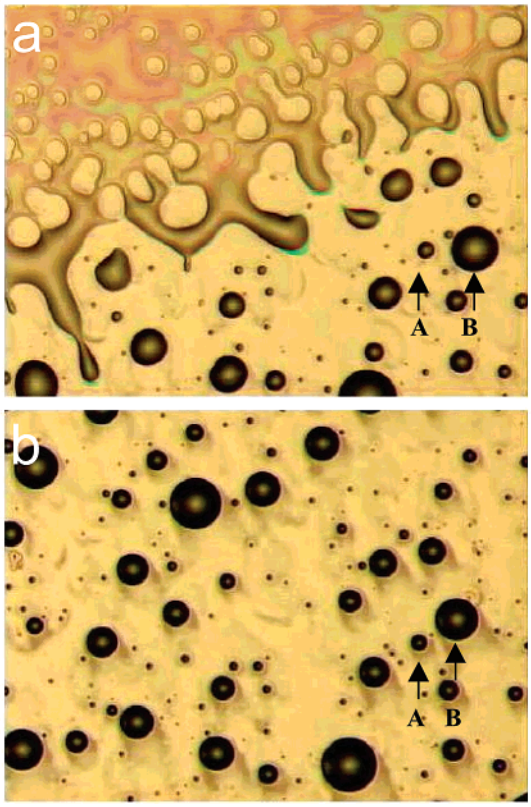

Figure 11. An optical image of the region behind the dewetting front in a OEP/hOS mixture ($\phi_{OEP} = 0.5$). The image is 0.25 × 0.25 mm. (a) Formation of droplets due to Rayleigh instabilities. (b) An image of the same region 8 h later indicates that the OEP droplets (see for example the drop marked A) have moved (in the direction of the arrow) a distance of about 10 microns, leaving behind tracks of deformed liquid. The scale bar is 100 μm. Note that larger droplets move faster: thus in (a) droplet A is at the same position as droplet B, but in image (b), 8 h later, the larger droplet B had moved well ahead of the smaller droplet A.

the cessation of dewetting of the liquid upper layer when the lower layer becomes glassy and solid: the solid substrate does not allow the propagation of the crest, and consequently local thinning of the upper liquid film does not take place and the process is quenched.

Following the formation of holes and their subsequent growth, we observe the development of a characteristic finger structure as can be seen in Figure 11a. Rayleigh instabilities[22] lead to a further breakup of the liquid cylinders, resulting in the array of droplets of various sizes in the dewetted region (Figure 11b). Despite the finite viscous dissipation at the droplet/substrate interface, these droplets continue to move toward the center of the sample for more than a day. We believe this is due to a lateral composition gradient which results in a gradient in the interfacial tension from the sample edges inward, as earlier discussed for the front propagation motion. A simple analysis[25] suggests that larger droplets should move faster than smaller ones, as we indeed observed; see

(25) For a droplet of height h_d and radius of contact r with the underlying liquid substrate, the force in the x direction, towards the center, is $F_d \cong \pi r^2(\partial\gamma/\partial x)$, where $\partial\gamma/\partial x$ is the gradient in surface energy arising from the dewetting. Assuming the inertial term is negligible, the viscous dissipation rate for a droplet moving at velocity v_d is approximately $(v_d/h_d)^2\eta^*$(drop volume) $\cong (v_d/h_d)^2\eta(\pi r^2 h_d)$. Equating the work done on the drop in time Δt, due to motion Δx, to the dissipation in that time, we have $F_d\Delta x = F_d v_d \Delta t = \pi r^2(\partial\gamma/\partial x)v_d\Delta t = (v_d/h_d)^2\eta(\pi r^2 h_d)\Delta t$, giving $v_d \cong (h_d/\eta)(\partial\gamma/\partial x)$, i.e., that larger drops (larger h_d and therefore larger r) should move faster, as indeed they are observed to do.

for example Figure 11a,b. An ongoing investigation of the persistent droplet motion will be the subject of a future publication.

To conclude, we observed that a thin liquid film of a binary liquid mixture, which is metastable with respect to both the chemical composition and the interfacial energy, may relax by phase separation and dewetting. The latter process is characterized by the formation of a liquid front leading to an accelerated dewetting. We suggest that the origin of this pathway is a Marangoni flow induced by spatial gradients of surface energy, followed by the motion of a dewetting front which propagates rapidly by inducing rupture of the liquid ahead of it. The process is believed to be general and important in thin films of partially miscible liquid mixtures.

Acknowledgment. R. Y.-R. gratefully acknowledges The Joseph and May Winston Foundation Career Development Chair in Chemical Engineering and The Ilse Katz center for Meso and Nano-Scale Science and Technology for their support. J.K. thanks Robin Ball and Tom Witten for illuminating discussions, Matti Oron for useful comments, and the German-Israel Foundation (GIF), the US-Israel Binational Science Foundation (BSF), and the Minerva Foundation for support of this work.

LA0203178